Available online at www.sciencedirect.com

ScienceDirect

IFAC Papers Online CONFERENCE PAPER ARCHIVE

IFAC PapersOnLine 59-33 (2025) 93–98

Adaptive Pure Pursuit NMPC for Autonomous Mooring of Inland Cargo Vessels ⋆

J. G. Martin * **Y. Pang** * **D. Schott** *

* *Department of Maritime and Transport Technology, Faculty Mechanical Engineering, Delft University of Technology, Mekelweg 2, 2628 CD Delft, the Netherlands (e-mail: y.pang@tudelft.nl)*

AbstractInland shipping is a key component of transport infrastructure, as it provides an energy-efficient and cost-effective method for moving goods. This report aims to investigate how an autonomous mooring system for inland cargo vessels can be modeled and evaluated, to improve efficiency and safety during mooring operations. This study develops a vessel model that simulates relevant mooring behaviours under varying environmental conditions and designs a control system for accurate approach and successful mooring. Simulation results are analysed, focusing on approach accuracy and position-holding.

Keywords: Autonomous Mooring, Inland Cargo Vessels, Autonomous Surface Vehicles, Model Predictive Control.

1. INTRODUCTION

Inland shipping plays a vital role in the transport infrastructure of many countries, offering an energy-efficient and cost-effective means of moving goods. For instance, inland transport in the Netherlands alone accounts for 43% of all transport, highlighting its significant contribution to the country's logistics (Jacobs, 2022). As the demand for sustainable logistics increases, the development of autonomous inland vessels has become a focal point of innovation in maritime technology.

Recent studies remain focused on navigation and collision avoidance, for intance, in (Wang et al., 2020) a comprehensive review of motion-prediction, conflict detection, and resolution methods for manned and unmanned navigation is delivered; and in (Menges and Rasheed, 2024) a multi-level digital twin framework enabling predictive and autonomous decision-making for ASVs is proposed. Meanwhile, mooring, which is a key open challenge in MPC applications for marine autonomy (Wei and Shi, 2023), has seen limited but growing attention: in (Martinsen et al., 2019) docking is modelled as an optimal-control task and real-time MPC is demonstrated on a supply vessel; in (Kockum, 2022) precision docking of the USV Piraya under disturbances with an MPC controller is achieved; in (Jagernath, 2024) MPC across un-mooring, transit, and mooring phases on a scaled inland-vessel model is applied, keeping trajectory-errors under 10% of length. In (Homburger et al., 2022) Model Predictive Path Integral control on a fully-actuated vessel is used, yielding smooth maneuvers in field tests; in (Vijayakumar et al., 2025) MPPI is integrated with real-time LiDAR to validate safe dockings from varied starting points; and in(Larsen et al., 2024) an extended dynamic-positioning scheme validated experimentally on coastal ferries under disturbances is proposed. Without the ability to dock independently, unmanned vessels will continue to rely on human assistance during mooring operations, thereby limiting their autonomy, scalability, and cost-efficiency. Mooring remains a delicate maneuver in confined environments, requiring accuracy and controllability. Advances in predictive path-following control show that treating the progression along a geometric path as an optimisation variable can greatly improve accuracy in confined maneuvers (Faulwasser and Findeisen, 2009; Faulwasser et al., 2016). Related work in adaptive Pure Pursuit controllers shows that making the look-ahead distance a function of the remaining path length also yields finer spatial sampling and an implicit deceleration close to the goal (Ahn et al., 2021; Wang et al., 2025; Park et al., 2014). Building on this idea, a Non-linear Model Predictive Control (NMPC) framework is introduced, whose reference governor computes, at every sampling instant, the closest point on a spline-interpolated route and assigns a surge-velocity profile that decays smoothly with the remaining chord-length distance to the quay. As a result, reference way-points inside the prediction horizon become denser as the vessel nears the berth, giving the NMPC finer spatial resolution while naturally enforcing anticipative deceleration in an adaptive pure-pursuit fashion. Similar velocity-aware path-tracking concepts have so far been explored only for ground vehicles (Abdelaal and Schön, 2020).

The rest of this work is organized as follows: Section 2 describes the dynamic model of the inland vessel, including the assumptions, environmental disturbances, and relevant forces affecting mooring behaviour. Section 3 introduces key features on the control system, compares different motion control approaches, and presents the selected control system design. Section 4 outlines the simulation setup, defines key performance indicators, and evaluates the system under various environmental conditions. Section 5 presents the main conclusions and offers recommendations for future development.

2. PROBLEM FORMULATION

In the first place, we consider an inland cargo vessel modeled after a typical CEMT II class 'Kempenaar' (Koedijk, 2020), characterized by an *over-actuated* propulsion system, i.e., a fully rotatable azimuth thruster and a bow-mounted tunnel thruster. The main aim is to perform the docking maneuver

⋆ This work has been supported by the European Union's Horizon 2020 research and innovation programme, project MAGPIE.

10.1016/j.ifacol.2025.12.428

autonomously. Thus, low-speed conditions can be assumed, and the 3 degrees of freedom model from (Fossen, 2011), disregarding Coriolis effect and considering linear damping, can be used:

$$\dot{\eta} = R(\varphi)\nu_r, \tag{1}$$
$$\dot{\nu}_r = M^{-1}(\tau + \tau_{\text{wind}} - D_L\nu_r), \tag{2}$$
$$\nu_r = \nu - R(\varphi)^{\mathsf{T}}\nu_c, \tag{3}$$

where $\eta = [x\ y\ \varphi]^{\mathsf{T}}$ are the global coordinates of the vessel's center of gravity (CoG), and the heading angle respect to the absolute frame, $\nu = [u\ v\ r]^{\mathsf{T}}$ is the velocity vector in the vessel frame, $R(\varphi)$ the rotation matrix, ν_c is the water current in the absolute frame, τ represent the forces and moments produced by the thrusters. Furthermore, $\tau = [\tau_u\ \tau_v\ \tau_r]^{\mathsf{T}}$, with $\tau_u = F_T\cos\alpha$, $\tau_v = F_B + F_T\sin\alpha$, and $\tau_r = l_T F_T\sin\alpha + l_B F_B$. Note F_T and F_B are the azimuth and bow thruster forces respectively, α is the azimuth angle, and l_T and l_B are the longitudinal offsets from the CoG to each thruster. Matrix $M \in \mathbb{R}^{3\times3}$ and $D_L \in \mathbb{R}^{3\times3}$ are the total inertia matrix and the linear damping matrix and take the following form:

$$M = \begin{bmatrix} m - X_{\dot{u}} & 0 & 0 \\ 0 & m - Y_{\dot{v}} & -Y_{\dot{r}} \\ 0 & -N_{\dot{v}} & I_z - N_{\dot{r}} \end{bmatrix},\ D_L = \begin{bmatrix} X_u & 0 & 0 \\ 0 & Y_v & Y_r \\ 0 & N_v & N_r \end{bmatrix}.$$

Finally, τ_{wind} represents the steady wind forces and the yaw moment on the vessel an can be expressed as

$$\tau_{\text{wind}} = \tfrac{1}{2}\rho V_{wr}^2 \begin{bmatrix} -c_x\cos(\gamma_w)A_x \\ c_y\sin(\gamma_w)A_y \\ c_n\sin(2\gamma_w)A_y L_{\text{OA}} \end{bmatrix} \tag{4}$$
$$\mathbf{v}_{wr} = R(\varphi)^{\mathsf{T}}\big(\mathbf{v}_a - \mathbf{v}_n\big), \tag{5}$$
$$V_{wr} = \|\mathbf{v}_{wr}\|,\ \gamma_w = \angle\mathbf{v}_{wr} - \varphi. \tag{6}$$

where $\mathbf{v}_a$ is the wind velocity vector in absolute frame, $\mathbf{v}_n = [u\ v]^{\mathsf{T}}$, A_x, A_y are the projected frontal and lateral wind-exposed areas and L_{OA} is overall length, and the coefficients ranges ($c_x \in [0.50, 0.90]$, $c_y \in [0.70, 0.95]$, $c_n \in [0.05, 0.20]$) are obtained from (Fossen, 2011). Note that ports are often enclosed or equipped with breakwaters that significantly reduce wave activity, resulting in relatively calm water conditions. As a consequence, modelling efforts for autonomous operations such as mooring can reasonably neglect wave-induced forces.

Finally, the presence of robotic mooring arms is assumed on board of the inland cargo vessel. These robotic arms are responsible for physically connecting the mooring lines to bollards once the vessel is positioned correctly during docking. Neither the modelling nor the control of the robotic arms is included in this work; they are assumed to operate reliably once the vessel is within a predefined positional tolerance near the quay. Therefore, the objective of the control system is to guide the vessel to the designated docking position with zero translational velocity and an orientation aligned with the quay. Once in position, the vessel must remain sufficiently stationary for a specified duration to enable the successful execution of the mooring procedure by robotic arms. This requirement imposes strict constraints on both the final approach and the station-keeping phases of the maneuver.

3. CONTROL METHOD

3.1 Non-linear Model Predictive Control

Predictive control can explicitly handle system constraints and predict future behavior, making it well suited for real-time control applications with practical implementability. However, given the non-linear dynamics inherent in vessel motion, non-linear control better captures system complexities and improves robustness and accuracy, offering a superior trade-off between performance and model fidelity for this application. NMPC predicts the future evolution of the system based on its current state, an estimation of the vessel dynamics and environmental disturbances, and computes control actions that minimize a cost function, while simultaneously satisfying system constraints. At every sampling instant k, the NMPC controller receives the vessel's current state vector $\mathbf{x}(k) = [x(k)\ y(k)\ \varphi(k)\ u(k)\ v(k)\ r(k)]^{\mathsf{T}}$, and uses it to predict the effect of different control actions $\mathbf{u}(k) = [F_T(k)\ F_B(k)\ \alpha(k)]^{\mathsf{T}}$. The optimizer must ensure accurate tracking of the reference trajectory while enforcing smooth actuator commands, avoiding large jumps in actuator forces or azimuth thruster angle changes, i.e., it must solve the following problem over a prediction horizon N_p:

$$\begin{aligned} \min_{\mathbf{U}}\quad & J_k(\mathbf{U}) = \sum_{i=0}^{N_p} \mathbf{e}(k+i|k)^{\mathsf{T}}\mathbf{Q}\mathbf{e}(k+i|k) \\ & \qquad + \Delta\mathbf{u}(k+i|k)^{\mathsf{T}}\mathbf{S}\Delta\mathbf{u}(k+i|k), \\ \text{s.a.}\quad & x(k+i+1|k) = f_{\mathbf{RK}}(x(k+i|k), u(k+i|k)), \\ & i = 0,\dots,N_p-1 \\ & \mathbf{e}(k+i|k) = \mathbf{x}(k+i|k) - x_r(k+i), \\ & \Delta\mathbf{u}(k+i|k) = \mathbf{u}(k+i|k) - \mathbf{u}(k+i-1|k), \\ & \mathbf{u}_{\min} \le \mathbf{u}(k+i) \le \mathbf{u}_{\max},\ i = 0,\dots,N_p-1, \\ & \Delta\mathbf{u}(k+i) \le \Delta\mathbf{u}_{\min},\ i = 0,\dots,N_p-1, \end{aligned} \tag{7}$$

where $\mathbf{U} = [u(k)\ u(k+1)\ \dots\ u(k+N_p)]^{\mathsf{T}}$, i.e., the aggregated vector of control actions over the prediction horizon, $f_{\mathbf{RK}}(.)$ is the Runge–Kutta discretization of the continuous model in (1)–(6) with sampling time T_s, $\mathbf{x}(k|k) = \mathbf{x}(k)$, and $\Delta\mathbf{u}(k|k)$ is computed using the last applied input $\mathbf{u}(k-1)$. Note that the first term of the cost function penalizes state deviation from the reference, and the second penalizes input changes. The diagonal matrix $Q \in \mathbb{R}^{6\times6}$ and $S \in \mathbb{R}^{3\times3}$ set each component's weight. Larger values impose stronger penalties, directing the optimizer to focus on reducing that particular state deviation or smoothing the corresponding control change. Once, the optimizer computes an optimal control sequence that satisfies the constraints, it only applies the input $\mathbf{u}^\star(k|k)$, updates the state at $k+1$, and then repeats the process in a receding-horizon fashion.

3.2 Reference Governor

The reference trajectory is precomputed based on manually selected GPS waypoints, i.e., let the ordered way-points be

$$w_i = (x_i, y_y) \in \mathbb{R}^2, \quad i = 0,1,\dots,N, \tag{8}$$

and denote the successive chord lengths by

$$d_i := ||w_i - w_{i-1}||, \quad i = 1,\dots,N, \tag{9}$$

with

$$L := \sum_{i=1}^{N} d_i > 0. \tag{10}$$

Set the normalized cumulative chord-length parameter

$$s_0 = 0, \quad s_i = \frac{1}{L}\sum_{j=1}^{i} d_j, \quad i = 1,\ldots,N, \tag{11}$$

so that each increment $s_i - s_{i-1}$ is proportional to the Euclidean distance between consecutive points. Let us also define the component functions $x, y : [0,1] \to \mathbb{R}$, as the unique cubic splines of class C^2 that interpolate the data sets (s_i, x_i) and (s_i, y_i). Then, the resulting geometric path is the parametric map $r : [0,1] \to \mathbb{R}^2, \quad r(s) = [x(s), y(s)]$, whose image $\mathscr{R} := r([0,1])$ is a C^2 curve passing smoothly and exactly through every waypoint at a proportional to the physical distance traveled along consecutive segments. Let also $p(k) = [x(k), y(k)]^\mathsf{T} \in \mathbb{R}^2$ be the position of the vessel at instant k. The closest-point parameter is

$$s^\star(k) := \arg\min_{s\in[0,1]} ||r(s) - p(k)||^2, \tag{12}$$

and the closest point on the path is $\hat{r}(k) := r(s^\star(k)) \in \mathscr{R}$. Let us now define $d(k)$ as the chord-distance from the closest point from the vessel to the docking position, i.e.,

$$d(k) := L(1 - s^\star(k)). \tag{13}$$

Since the vessel is performing a docking maneuver, let us also define a desired surge speed during the operation as

$$u_d = \begin{cases} u_c, & d(k) \geq L_d, \\ \min(u(k), u_c \cos(\frac{\pi}{2}\frac{(L_d - d(k))}{L_d})), & \delta > d(k) > L_d, \\ 0, & d(k) \leq \delta, \end{cases} \tag{14}$$

being L_d a parameter that defines where the vessel needs to start braking, δ a tolerance from which we consider the vessel must remain stopped, and u_c the cruise speed within the port. Thus, the extended reference for the NMPC in the prediction horizon N_p is obtained recursively from the closest-point parameter $s^\star(k)$. Let

$$v_c(s) := ||r'(s)|| = \sqrt{\dot{x}(s)^2 + \dot{y}(s)^2}, \tag{15}$$

be the geometric speed of the path. Then, starting from $s_k \equiv s^\star(k)$ we propagate a virtual-time update

$$s_{k+j} = \min(s_{k+j-1} + \frac{u_d(k+j-1)}{v_c(s_{k+j-1})} T_s, 1), \; j = 1,\ldots,N_p, \tag{16}$$

which advances the path parameter by the Euclidean distance that the vessel is expected to travel in one control step, scaled by the local metric of the curve. The prediction-horizon reference reads

$$x_r = \begin{bmatrix} \hat{r}(s_{k+j}) \\ \text{atan2}(\dot{y}(s_{k+j}), \dot{x}(s_{k+j})) \\ u_d(k+j) \\ 0 \\ 0 \end{bmatrix}, \quad j = 0,\ldots,H. \tag{17}$$

In simple terms, at each control step, we locate the point on this curve closest to the current position and then "roll forward" along the curve by the distance the vessel is expected to travel in one sampling period. How far we move along the curve depends on the desired surge speed at that instant, which itself is set by how far we are from the final docking position (slower as we approach).

4. SIMULATION

4.1 Problem setting

The NMPC prediction model and the simulation both employ the identical non-linear 3-DOF vessel dynamics from Eq. (1)-(6). The difference is in the integration time step: inside the NMPC optimizer, states are propagated over each sampling interval $T_s^{\text{MPC}} = 0.8\ s$, whereas in the simulation (or real-time implementation), the same dynamics update at every $T_s^{\text{dyn}} = 0.4\ s$ to advance the plant. Length $L_{\text{decel}} = 60\ m$ is used to determine the deceleration zone and length $\delta = 0.014\ m$ the holding tolerance. Speed $u_c = 2\ m/s$ is used to define the cruise surge speed. Throughout all phases, the reference sway speed and yaw rate remain fixed at zero). Next, the diagonal state-weighting matrix is $\mathbf{Q} = \text{diag}(10^6,\ 10^6,\ 10^8,\ 0,\ 0,\ 0)$, and the input-increment weight matrix is $\mathbf{S} = \text{diag}(10^3,\ 10^3,\ 10^6)$. Note that there is no need of weighting error in velocities since the references in position are already accounting for desired velocities. The constraint boundaries are specified in Table 1, including both input bounds on thruster forces and azimuth angle, and rate limits on azimuth angle changes (Fossen and Perez, 2004).

Table 1. NMPC Constraints

Constraint	Value
F_T	$[-7\times10^5,\ 7\times10^5]$ N
F_B	$[-1.5\times10^5,\ 1.5\times10^5]$ N
α	$[-\pi,\ \pi]$ rad
$\lvert\Delta\alpha\rvert$	$\leq 15^\circ\,\text{s}^{-1}$

Measurements of wind, current, and vessel states are assumed ideal. As a result, the estimations provided to the NMPC are identical to the true values used in the simulation (or real-time implementation). This implies that all external disturbances acting on the vessel are fully known to the predictor, and no unmeasured disturbances enter the optimization process. Also, both the wind and current are varied to simulate three different environmental conditions. Table 2 shows the three scenarios, starting with no wind or current. The disturbances mild and heavy are representative of common scenarios, with realistic values. To extend the validation of results, the wind and current directions are randomly varied across simulations. The mean performance is then calculated for each scenario.

Table 2. Environmental-Disturbance Scenarios

Scenario	Wind [m/s]	Current [m/s]
No Disturb.	0.00	0.00
Mild Disturb.	10.00	1.00
Heavy Disturb.	20.00	2.00

4.2 Key Performance Indicators

To assess the performance of the autonomous mooring controller, three key performance indicators (KPIs) are defined. The KPIs are chosen to obtain both the accuracy of the approach trajectory, using cross-track error and heading error, and the reliability of the mooring. The vessel state is logged at each step, and all three KPIs are computed for evaluation.

First, the cross-track error (CTE) measures lateral deviation from the path. Second, the heading error (HE) consider the difference between the reference heading and the actual heading. Both values are examined at step k:

$$\begin{aligned} \mathrm{CTE}(k) =& -(\mathbf{x}(k)-x_r(k))\sin(\varphi_r(k)) \\ &+(\mathbf{y}(k)-y_r(k))\cos(\varphi_r(k)), \end{aligned} \tag{18}$$

$$\mathrm{HE}(k) = \varphi(k)-\varphi_r(k). \tag{19}$$

The metrics $\overline{|\mathrm{CTE}|}$ (average lateral offset) and $\max\{|\mathrm{CTE}|\}$, $\overline{|\mathrm{HE}|}$, and $\max\{|\mathrm{HE}|\}$, are reported over the approach phase.

Finally mooring success (MS) is evaluated during the hold phase ($t > T_f$). During this phase the positions of the two mooring-arm end-points are tracked, extending from the vessel's centerline by longitudinal offsets $l_{M,A}$ and $l_{M,B}$. Their coordinates are:

$$\begin{aligned} A_k &= \begin{bmatrix}\mathbf{x}(k)\\ \mathbf{y}(k)\end{bmatrix} + \begin{bmatrix}\cos(\varphi(k)) & -\sin(\varphi(k))\\ \sin(\varphi(k)) & \cos(\varphi(k))\end{bmatrix}\begin{bmatrix}l_{M,A}\\ 0\end{bmatrix} \\ B_k &= \begin{bmatrix}\mathbf{x}(k)\\ \mathbf{y}(k)\end{bmatrix} - \begin{bmatrix}\cos(\varphi(k)) & -\sin(\varphi(k))\\ \sin(\varphi(k)) & \cos(\varphi(k))\end{bmatrix}\begin{bmatrix}l_{M,B}\\ 0\end{bmatrix} \end{aligned} \tag{20}$$

Here, A_k and B_k represent the instantaneous locations of the bow and stern mooring-arm hooks. For autonomous mooring to succeed, each hook must fall within a circular reach region of radius r_{reach} around its corresponding bollard at positions A_{bollard} and B_{bollard}. Furthermore, both absolute distances A_k and B_k from the A_{quay} and B_{quay} need to remain above the s_{safety}. Thus, a time step is counted as successful if:

$$\begin{aligned} \left\|A_k - A_{\text{bollard}}\right\| \;\&\; \left\|B_k - B_{\text{bollard}}\right\| &\le r_{\text{reach}} \\ \left\|A_k - A_{\text{quay}}\right\| \;\&\; \left\|B_k - B_{\text{quay}}\right\| &\ge s_{\text{safety}} \end{aligned} \tag{21}$$

The *mooring success* is passed if all sets of coordinates are considered successful.

4.3 Results and Discussion

First, we present the results of a representative simulation under heavy disturbances (see Fig. 1), which can be viewed in full here. The solid blue line shows the actual trajectory followed by the barge, while the dashed red line represents the desired path. It can be observed that the barge closely tracks the intended trajectory.

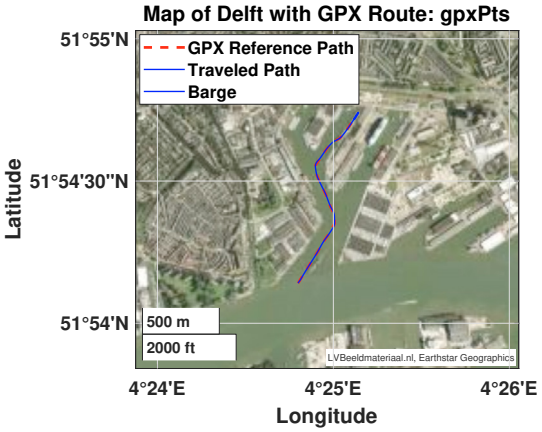

Figure 1. Traveled route by the vessel.

Furthermore, Fig. 2 displays the control actions computed for the vessel, which are smooth throughout the operation, and shows that sway motion remains very limited, and the yaw rates are gentle. The surge velocity stays close to the desired cruise speed for most of the journey, decelerating smoothly from the predefined deceleration distance.

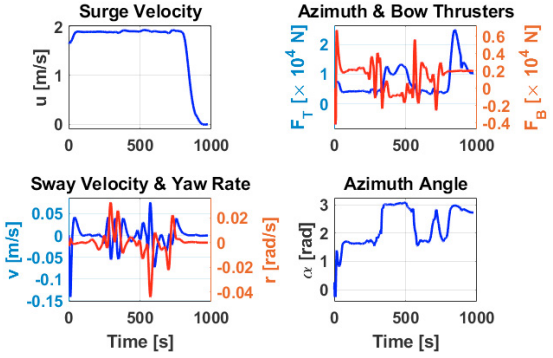

Figure 2. Vessel velocities and control actions during heavy disturbance simulation.

During the approach phase, CTE and HE are used to assess the accuracy of the trajectory under varying environmental conditions. Table 3 summarizes the results for each disturbance scenario among 30 simulations of each type.

Table 3. Results approach phase

Criteria	Scenario		
	No	Mild	Heavy
Max. CTE [m]	1.0307	1.1549	1.8392
Avg. CTE [m]	0.1544	0.2320	0.4496
Max. HE [°]	0.1193	0.1281	0.2900
Avg. HE [°]	0.0143	0.0147	0.0158

The results illustrate that increasing wind and current disturbances lead to higher values of both CTE and HE. The average CTE increases from 0.1544 m in the no-disturbance case to 0.4496 m under heavy conditions. This corresponds to approximately 0.82% of the vessel's length ($LOA = 55\ m$), indicating that the controller maintains an accurate trajectory throughout the approach. The difference between the mild and heavy cases

is limited, the largest increase in deviation occurs between the mild and heavy disturbance scenarios. The average HE increases from 0.0143° to 0.0158°, showing that the vessel remains closely aligned with the reference orientation, even under environmental influence. As can be seen in Fig. 3, the heading errors rarely goes over 1° across all scenarios indicating small orientation deviations during the approach phase. Also, the maximum values of CTE and HE are substantially higher than the averages. These peaks are primarily observed during turns in the reference trajectory, where sharper control actions are required. These local increases are expected, as turning maneuvers demand larger lateral and rotational adjustments that are influenced by the system constraints. Interestingly, across all environmental disturbance scenarios, the CTE profiles follow a similar shape over time. This consistency indicates that the propsed method is stable and reliable across a range of external conditions. While the magnitude of the deviations increases with disturbance intensity, the CTE profile remains nearly unchanged.

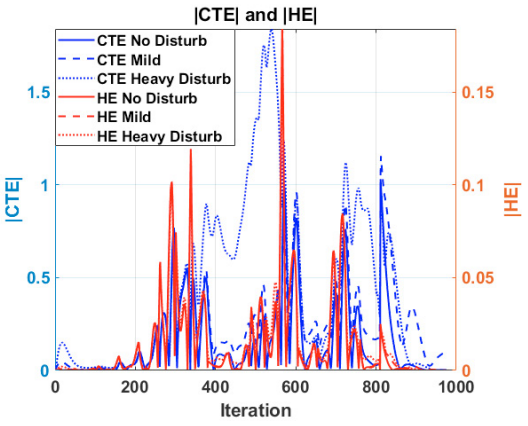

Figure 3. Mean absolute HE during the approach phase

During the hold phase, the vessel's mooring position is recorded every 0.8 seconds and evaluated against the mooring criteria defined in Eq. (21) with $r_{\text{reach}} = 15\ m$ and $s_{\text{safety}} = 6\ m$. These criteria verify whether both mooring points remain within the defined reach regions of their respective bollards while maintaining a safe distance from the quay. Figure 4 visualises the vessel's position and alignment during the hold phase, including the reach boundaries, safety margins, quay line, and the outline of the vessel.

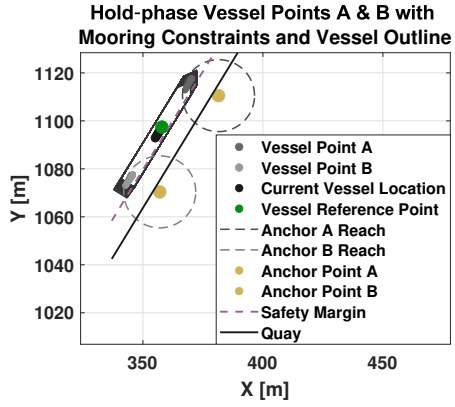

Figure 4. Mooring position through time

The results for all disturbance scenarios are shown in Table 4. In each simulation, the vessel successfully met the mooring criteria at every time step, with zero failures observed across 30 evaluations per scenario, meaning the *mooring success* is passed in all cases. The vessel consistently maintained its final position within the required tolerance bounds under all environmental conditions. This indicates that, once the vessel reaches the mooring region, the controller is able to hold position in a manner that satisfies the spatial constraints of the mooring system. The absence of failures across all tested cases highlights that the controller maintains both mooring points within the required bounds at every time step. Given the vessel's size and the presence of wind and current disturbances, achieving zero failures throughout the entire hold phase is a strong indication of consistent spatial performance under the defined mooring criteria.

Table 4. Mooring Feasibility Results

Criteria	Scenario		
	No	Mild	Heavy
Amount of successes	30	30	30
Amount of fails	0	0	0
Mooring success (MS)	Pass	Pass	Pass

The simulations has been performed using an MATLAB Intel(R) Core(TM) i7-1365U CPU with 1.80 GHz processor.The time required to compute the reference is negligible compared to the NMPC computation time and the overall average time per iteration is 0.69 seconds, which is below the selected sampling time for the NMPC, 0.8 seconds.

5. CONCLUSION

This work has developed and validated a high-fidelity method for autonomous mooring of inland cargo vessels based on NMPC. Through extensive MATLAB simulations, it was demonstrated that the developed method reliably converges to a stabilizing control action under three disturbance regimes. In the absence of wind and current, both lateral and heading errors remained within tight tolerances. When subjected to mild disturbances performance degraded marginally, with a slight increase in cross-track deviation but negligible impact on heading alignment. Even under heavy disturbances the controller continued to drive the vessel toward the quay without instability, although lateral error grew larger. These findings indicate that, while extreme environmental loads increase positional error, they do not cause the NMPC to lose stability or fail. Real-world deployment will involve measurement of noise, actuation delays, and hydrodynamic effects not captured by the current model (e.g., bank influence or wave action). Still, the present results establish a solid baseline: under moderate inland waterway conditions, the NMPC framework reliably guides the vessel into the mooring corridor with minimal human input. Future work will narrow the gap between simulation and practice by enhancing realism and implementation readiness. Key steps include replacing manual GPS waypoints with automated path planning to reduce wind and current effects while optimizing energy use, modeling environmental forces as time-varying inputs, and introducing sensor noise and thruster delays to test controller robustness. Finally, scaled lab experiments will validate the framework under controlled yet representative conditions.

ACKNOWLEDGEMENTS

The research presented in this paper was carried out as part of the MAGPIE project funded by the European Union's Horizon 2020 (MFF 2014 – 2020) research and innovation programme under Grant Agreement 101036594.

REFERENCES

Abdelaal, M. and Schön, S. (2020). Predictive path following and collision avoidance of autonomous connected vehicles. *Algorithms*, 13(3), 52.

Ahn, J., Shin, S., Kim, M., and Park, J. (2021). Accurate path tracking by adjusting look-ahead point in pure pursuit method. *International journal of automotive technology*, 22(1), 119–129.

Faulwasser, T. and Findeisen, R. (2009). Nonlinear model predictive path-following control. In *Nonlinear Model Predictive Control: Towards New Challenging Applications*, 335–343. Springer.

Faulwasser, T., Weber, T., Zometa, P., and Findeisen, R. (2016). Implementation of nonlinear model predictive path-following control for an industrial robot. *IEEE Transactions on Control Systems Technology*, 25(4), 1505–1511.

Fossen, T.I. and Perez, T. (2004). Marine systems simulator (mss). URL https://github.com/cybergalactic/MSS. Accessed: 2023-06-03.

Fossen, T.I. (2011). *Handbook of Marine Craft Hydrodynamics and Motion Control*. Wiley.

Homburger, H., Wirtensohn, S., and Reuter, J. (2022). Docking control of a fully-actuated autonomous vessel using model predictive path integral control. In *2022 European Control Conference (ECC)*, 755–760. IEEE, London, United Kingdom. doi:10.23919/ECC55457.2022.9838005. URL https://ieeexplore.ieee.org/document/9838005.

Jacobs, K. (2022). Inland waterway transport in the eu. Available at https://www.eprs.ep.parl.union.eu/.

Jagernath, R.W. (2024). *Autonomous Mooring and Unmooring with use of a Model Predictive Control Strategy*. Msc thesis, Delft University of Technology, Faculty of Mechanical Engineering, Department of Maritime and Transport Technology, Delft, Netherlands. Public defense: October 9, 2024. Student ID: 4713842. MSc track: Multi-Machine Engineering. Available at http://repository.tudelft.nl/.

Kockum, S. (2022). *Autonomous Docking of an Unmanned Surface Vehicle using Model Predictive Control*. Msc thesis, Lund University, Department of Automatic Control, Lund, Sweden. ISSN 0280-5316.

Koedijk, O.C.E. (2020). *Richtlijnen Vaarwegen 2020*. Rijkswaterstaat Dienst Water, Verkeer en Leefomgeving, 2 edition.

Larsen, S., Helgesen, H.H., Walmsness, J.E., Kufoalor, G.K.M., and Johansen, T.A. (2024). Automatic docking with extended dynamic positioning. *Journal of Marine Science and Technology*, 29(4), 770–788.

Martinsen, A.B., Lekkas, A.M., and Gros, S. (2019). Autonomous docking using direct optimal control. *IFAC-PapersOnLine*, 52(21), 97–102.

Menges, D. and Rasheed, A. (2024). Digital twin for autonomous surface vessels: Enabler for safe maritime navigation. *arXiv preprint arXiv:2411.03465*. URL https://arxiv.org/abs/2411.03465.

Park, M.W., Lee, S.W., and Han, W.Y. (2014). Development of lateral control system for autonomous vehicle based on adaptive pure pursuit algorithm. In *2014 14th international conference on control, automation and systems (ICCAS 2014)*, 1443–1447. IEEE.

Vijayakumar, A., A, A.M., and Somayajula, A. (2025). Model predictive path integral docking of fully actuated surface vessel. *arXiv preprint arXiv:2501.09668*. URL https://arxiv.org/abs/2501.09668. Submitted to arXiv on January 16, 2025.

Wang, X., Zhang, B., Du, X., Hu, X., Wu, C., and Cai, J. (2025). An adaptive path tracking controller with dynamic look-ahead distance optimization for crawler orchard sprayers. In *Actuators*, volume 14, 154. MDPI.

Wang, Z., Wang, Y., and Negenborn, R.R. (2020). Ship collision avoidance methods: State-of-the-art. *Reliability Engineering & System Safety*, 200, 106584. doi:10.1016/j.ress.2020.106584. URL https://www.sciencedirect.com/science/article/pii/S0925753519306356.

Wei, H. and Shi, Y. (2023). Mpc-based motion planning and control enables smarter and safer autonomous marine vehicles: Perspectives and a tutorial survey. *IEEE/CAA Journal of Automatica Sinica*, 10(1), 8–24. doi:10.1109/JAS.2022.106016. URL https://ieeexplore.ieee.org/document/9976181.